Chemical Science

RSC Publishing

EDGE ARTICLE

View Article Online
View Journal | View Issue

$Sc_2S@C_2(7892)$–C_{70}: a metallic sulfide cluster inside a non-IPR C_{70} cage†

Cite this: *Chem. Sci.*, 2013, **4**, 180

Ning Chen,‡[a] Marc Mulet-Gas,[b] Yu-Yang Li,[a] Riane E. Stene,[a] Curtis W. Atherton,[a] Antonio Rodríguez-Fortea,*[b] Josep M. Poblet*[b] and Luis Echegoyen*[a]

Received 28th July 2012
Accepted 6th October 2012

DOI: 10.1039/c2sc21101g

www.rsc.org/chemicalscience

A new cage isomer of C_{70}, $Sc_2S@C_2(7892)$–C_{70}, has been isolated and characterized by mass spectrometry, UV-Vis-NIR absorption spectroscopy, cyclic voltammetry and DFT calculations. The combined experimental and computational studies lead to the unambiguous assignment of the cage symmetry to $C_2(7892)$–C_{70}. The comparison between $Sc_2S@C_2(7892)$–C_{70} and related endohedral structures has been discussed. A close structural resemblance between $Sc_2S@C_2(7892)$–C_{70} and $Sc_2S@C_s(10\,528)$–C_{72} suggests that the conversion of these two molecules may be the result of a simple insertion of C_2 and the structural difference between $Sc_2S@C_2(7892)$–C_{70} and $Sc_3N@C_{2v}(7854)$–C_{70} shows that the nature and geometry of the encaged cluster plays an important role on the selection of the non-IPR cage.

Introduction

Fullerenes are spherical molecules composed of pentagons and hexagons.[1,2] Endohedral fullerenes, which possess outer surface available for chemical modification and inner space capable of encapsulation of variable clusters and molecules, have generated considerable recent research interest.[3,4] As a special class of endohedral fullerenes, clusterfullerenes (CFs) are known for their exceptionally high yield and fascinating structural versatility of the encapsulated clusters and carbon cages.[5–7] After the discovery of the first clusterfullerene in 1999, $Sc_3N@I_h$–C_{80},[8] nitride cluster fullerenes (NCFs),[9] carbide cluster fullerenes (CCFs),[10,11] oxide cluster fullerenes (OCFs)[12–14] and sulfide cluster fullerenes (SCFs)[15–17] were discovered and the encapsulated clusters were found to have a significant influence on the cage structure and their chemical reactivities.[18] With the remarkable versatility to alter their physical and chemical properties based on the structural variety of both cages and clusters, these molecules are attracting widespread interest in applications such as MRI agents and in molecular electronic devices and solar cells.[19–27]

Sulfide cluster fullerenes (SCFs) are the newest member in the CF families.[15,16] Different methods have been utilized to synthesize these compounds. Dunsch and co-workers reported the formation of one isomer of $M_2S@C_{82}$ (M = Sc, Lu, Dy) by introducing $CH_5N_3 \cdot HSCN$ as a solid sulfur source.[15] We demonstrated that an extensive family of novel scandium sulfide cluster fullerenes with cages ranging from C_{68} to C_{100} can be obtained in macroscopic quantities by introducing SO_2 into the arc reactor.[16] Further isolation and characterization of some of these new species revealed novel structures and properties which are unique to this family. Two isomers of $Sc_2S@C_{82}$, $Sc_2S@C_s(6)$–C_{82} and $Sc_2S@C_{3v}(8)$–C_{82}, were identified as the most abundant products in this family and were recently characterized by single crystal X-ray crystallography.[17] $Sc_2S@C_s(6)$–C_{82}, in particular, was found to possess completely ordered cage and cluster in its single crystal structure, the first in the clusterfullerene series.[17] Very recently, we reported the isolation of a metallic clusterfullerene in a non-IPR (Isolated Pentagon Rule) C_{72} cage, $Sc_2S@C_{72}$. Crystallography clearly established that the C_{72} cage has an unusual $C_s(10\,528)$ symmetry.[28] A combined computational and experimental study revealed that the unique geometry of the Sc_2S cluster together with a formal charge transfer of four electrons between the cluster and the cage play an important role in the stabilization of this new cage which had never been detected experimentally before in any of the CF families. These results indicate that more novel endohedral structures are likely to be found in the SCF family and systematic studies of these structures might provide a better understanding of the fundamental aspects of SCFs, and useful design principles to guide the preparation of high yielding endohedral compounds with unique and useful optoelectronic properties.

[a]*Department of Chemistry, University of Texas at El Paso, El Paso, Texas 79968, USA. E-mail: echegoyen@utep.edu; Fax: +1-915-747-8807; Tel: +1-915-747-7573*

[b]*Departament de Química Física i Inorgànica, Universitat Rovira i Virgili, c/Marcel·lí Domingo s/n, 43007 Tarragona, Spain. E-mail: josepmaria.poblet@urv.cat; antonio.rodriguezf@urv.cat; Fax: +34-977-559-563; Tel: +34-977-559-569*

† Electronic supplementary information (ESI) available: HPLC chromatograms and computational results (relative energies and plots of the structures for all the isomers computed in this work, schematic representation showing the relationship between $C_2(7892)$–C_{70} and $C_s(10\,528)$–C_{72} cages, and *xyz* coordinates for the lowest-energy computed isomers). See DOI: 10.1039/c2sc21101g

‡ Current address :College of Chemistry, Chemical Engineering and Materials Science, Soochow University, Suzhou, Jiangsu, 212163, China. Email: chenning@suda.edu.cn

Herein we report a new sulfide cluster fullerene, $Sc_2S@C_2(7892)$–C_{70}, in which the sulfide cluster is encapsulated inside a non-IPR C_{70} cage. This represents the third isomer of a C_{70} cage discovered to date. Combined computational and experimental studies lead to the unambiguous assignment of the cage symmetry to $C_2(7892)$–C_{70}.

Results and discussion

Preparation and characterization of $Sc_2S@C_{70}$

The SCFs were synthesized in a conventional Krätschmer–Huffman reactor using an atmosphere of helium and SO_2.[16,29] The as-produced soot was Soxhlet-extracted with CS_2 and a multi stage high-performance-liquid chromatography (HPLC) procedure was utilized to isolate and purify $Sc_2S@C_{70}$.

$Sc_2S@C_{70}$ is the second smallest fullerene in the SCF family after $Sc_2S@C_{68}$. The HPLC-MALDI TOF analyses show that on a 5PYE column, the $Sc_2S@C_{70}$ fraction overlaps with those of C_{76}, C_{78} and $Sc_2S@C_{72}$ (see Fig. 1). The retention time of $Sc_2S@C_{70}$ is shorter than that of $Sc_2S@C_{72}$, which agrees with the relatively smaller size of this compound. This fraction was further separated by a two-stage recycling HPLC procedure using a Buckyprep column, that resulted in the isolation of pure $Sc_2S@C_{70}$ (see ESI†). However, compared to the previously reported $Sc_2S@C_s(10\,528)$–C_{72}, a very similar non-IPR SCF in a small cage, the yield of this compound is much lower than that of $Sc_2S@C_s(10\,528)$–C_{72}. Out of the arcing processes of 60 packed graphite rods, along with 2.0 mg of $Sc_2S@C_s(10\,528)$–C_{72}, only 0.4 mg of $Sc_2S@C_{70}$ were obtained after HPLC purification.

The MALDI-TOF spectrum (Fig. 2) of the isolated fraction shows a single peak at 961.904. The isotopic distribution of the experimental MALDI spectrum shows excellent agreement with the corresponding theoretical spectrum (see Fig. 2). The purity of this sample was further checked by HPLC as shown in Fig. 1.

The purified $Sc_2S@C_{70}$ has a yellow-brown color in toluene solution. The UV-Vis-NIR absorption of $Sc_2S@C_{70}$ is shown in Fig. 3. A relatively strong absorption occurs at 1102 nm along

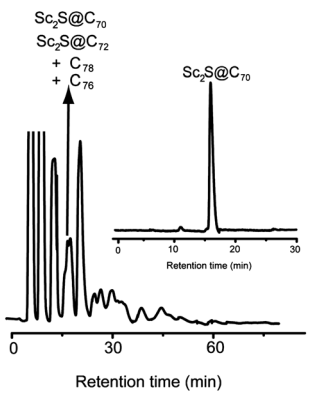

Fig. 1 HPLC Chromatograms of the fullerene extract obtained on a 10 mm × 250 mm 5PYE column using $\lambda = 320$ nm, a flow rate of 4 mL min^{-1}, and toluene as the eluent at 25 °C. Inset: HPLC of purified $Sc_2S@C_{70}$ obtained on a 10 mm × 250 mm 5PYE column using $\lambda = 320$ nm, a flow rate of 4 mL min^{-1}, and toluene as the eluent at 25 °C.

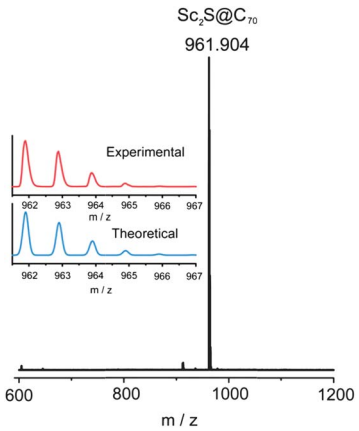

Fig. 2 Mass spectrum of the purified $Sc_2S@C_{70}$. Inset: the experimental and theoretical isotopic distribution for $Sc_2S@C_{70}$.

with other absorptions at 461, 634, 699 and 952 nm. The UV-Vis-NIR absorption spectrum of $Sc_2S@C_{70}$ shows some similarities to that of $Sc_2S@C_s(10\,528)$–C_{72}, which also features a strong absorption at 1076 nm around the absorption onset region, but is rather featureless in other spectral regions. The characteristic features of this spectrum are also substantially different from those of empty C_{70} and from those of the previously reported $Sc_3N@C_{2v}(7854)$–C_{70}, which presents the strongest absorption at 696 nm along with several shoulder peaks at 468, 558, 807 and 894 nm.[30] Since the absorption spectra of fullerenes in the visible and NIR region are dominated by the π–π* transitions of the carbon cages and the spectra are very sensitive to the carbon cage symmetries,[3] these differences clearly indicate that $Sc_2S@C_{70}$ has a non-IPR C_{70} cage and the cage symmetry is likely different from that of $Sc_3N@C_{2v}(7854)$–C_{70}.

The cyclic voltammogram (CV) of $Sc_2S@C_2(7892)$–C_{70} was recorded in *o*-dichlorobenzene (*o*-DCB) containing 0.05 M tetra(*n*-butyl)ammonium-hexafluorophosphate, (n-Bu_4NPF_6), as the supporting electrolyte using a scan rate of 100 mV s^{-1} (Fig. 4). The CV of $Sc_2S@C_2(7892)$–C_{70} shows some similarities and differences when compared to those of the other reported SCFs. The CV shows a reversible first oxidation followed by an irreversible second oxidation step, which is very similar to the oxidative behavior of $Sc_2S@C_s(10\,528)$–C_{72},[23] but different from those of the two isomers of $Sc_2S@C_{82}$, which exhibit two

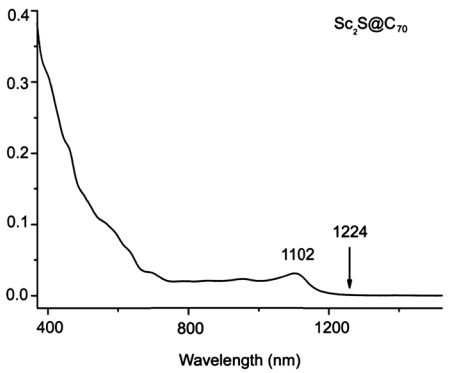

Fig. 3 UV-Vis-NIR absorption of $Sc_2S@C_{70}$ in CS_2 solution.

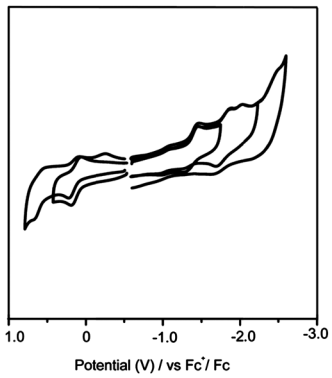

Fig. 4 Cyclic voltammograms of $Sc_2S@C_s(7892)$–C_{70} in n-Bu_4NPF_6/o-DCB with ferrocene as the internal standard; scan rate 100 mV s^{-1}.

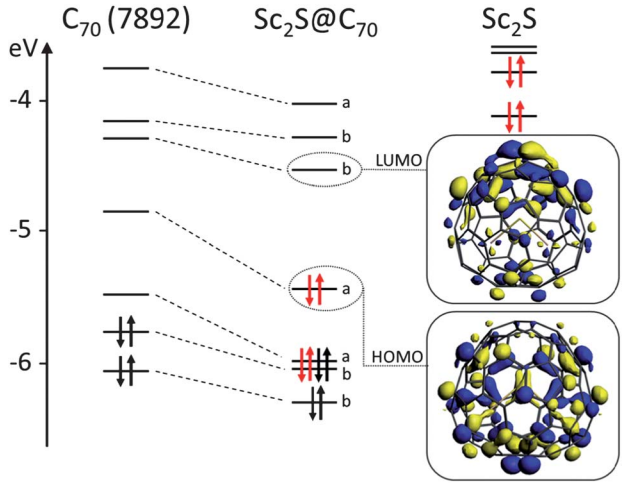

Fig. 5 Orbital interaction diagram for $Sc_2S@C_2(7892)$–C_{70}. The fragments, Sc_2S and $C_2(7892)$–C_{70}, were calculated with the same geometry they have in the clusterfullerene.

reversible oxidative steps.[16] On the other hand, while $Sc_2S@C_s(10\,528)$–C_{72} shows all-reversible reductive processes, the reductive behavior of $Sc_2S@C_2(7892)$–C_{70} shows similarities to those of the two isomers of $Sc_2S@C_{82}$ as well as to most of the cluster fullerenes, which typically exhibit irreversible reductive processes.[31]

The redox potentials of $Sc_2S@C_2(7892)$–C_{70} also show major differences from those of other reported SCFs. The first oxidation potential is shifted dramatically from 0.64 V for $Sc_2S@C_s(10\,528)$–C_{72}, to 0.14 V for $Sc_2S@C_2(7892)$–C_{70} (see Table 2).[28] This shows that $Sc_2S@C_2(7892)$–C_{70} is much easier to oxidize even though the cage sizes and topologies are very similar (see below). The electrochemical gap of $Sc_2S@C_2(7892)$–C_{70} is 1.57 V, which is smaller than that of $Sc_2S@C_s(10\,528)$–C_{72} (1.78 V) but somewhat larger than those of the corresponding $Sc_2S@C_{82}$ isomers (1.56 eV for $Sc_2S@C_{3v}(8)$–C_{82} and 1.47 eV for $Sc_2S@C_s(6)$–C_{82}).

Computational studies

Besides the experimental characterization of $Sc_2S@C_{70}$, we also performed an exhaustive computational study to assign the C_{70} cage symmetry among the 8149 possible isomers.§ From the electronic structure of the different computed isomers of $Sc_2S@C_{70}$, we verified that there is a formal transfer of four electrons, $(Sc_2S)^{4+}@(C_{70})^{4-}$, as for the other $Sc_2S@C_{2n}$ ($2n = 72$ and 82) known so far (see orbital interaction diagram, Fig. 5).[32,33] We have computed the energies of the tetraanions using DFT at BP86/TZP level for all 111 C_{70} cages with three or less adjacent pentagon pairs (APP): 1 IPR structure, 1 APP1, 18 APP2 and 91 APP3 (see ESI†). The SCF corresponding to the lowest-energy tetraanionic cages were also computed (a total of 17 isomers, Table 1).

Interestingly, the IPR cage, D_{5h}–$C_{70}(8149)$, was found to be the lowest-energy tetraanion. Other cage isomers with two and three APPs show relative energies within 10 kcal mol^{-1}. In particular, cage $C_2(7892)$–C_{70} exhibits the second most-stable tetraanion and is only 4 kcal mol^{-1} higher in energy than the IPR cage tetraanion (see Table 1). Among the 18 isomers with two pairs of fused pentagons, cage $C_2(7892)$–C_{70} shows the lowest number of pyracylene motifs and maximally separated pentagonal units (see ESI†).[34]

To predict the stability of a given clusterfullerene, it is necessary to consider electron transfer from the cluster to the cage but also the stability provided by the interaction between the metal atoms of the trapped cluster and the carbon cage. These interactions are not so critical for IPR cages; however, the cluster–cage interactions are crucial for those CFs that have one or more APPs. The systems with non-IPR cages are stabilized by the proximity of the metal cations of the cluster to the pentalene motifs, as in, for example, $Sc_3N@D_3(6140)$–C_{68},[36] $Gd_3N@C_s(39\,663)$–C_{82},[37] $M_3N@C_s(51\,365)$–C_{84} (M = Gd, Tm)[38] and the recently reported $Sc_2S@C_s(10\,528)$–C_{72}.[28] Thus, appropriate localization of the APPs on the fullerene cage that provide optimized interactions between the metal cations and the pentalene motifs is a *key* factor in the stabilization of non-IPR clusterfullerenes. In the present case, which resembles that of

Table 1 Relative energies (in kcal mol^{-1}) for several isomers of C_{70} in the tetraanion and endohedral forms[a,b]

Isomer	APP	C_{70}^{4-}	$Sc_2S@C_{70}$
8149	0	0.0	20.6
7892	2	3.9	0.0
7957	2	4.7	19.1
7851	3	6.2	20.3
7852	3	6.3	23.5
7887	3	7.0	21.6
7854	3	8.5	26.3
7893	3	9.4	19.7
7886	3	10.8	21.5
7924	2	11.6	18.6
7846	3	13.2	29.3
7960	2	14.1	21.9
7922	3	14.2	27.7
7921	3	14.7	29.1
7850	3	14.7	33.2
7847	3	15.6	28.8
8094	1	16.7	26.5

[a] Isomer number according to the spiral algorithm of Fowler and Manolopoulos.[35] [b] APP: number of adjacent pentagon pairs.

$Sc_2S@C_s(10\,528)$–C_{72},[28] it is only after the encapsulation of Sc_2S that the 7892–C_{70} cage becomes by far (~20 kcal mol^{-1}) the most stable endohedral isomer (Table 1). The most characteristic structural parameters, 2.352 Å for the Sc–S distance and 97.8° for the Sc–S–Sc angle, resemble those previously found for the two $Sc_2S@C_{82}$ isomers[19] and for $Sc_2S@C_s(10\,528)$–C_{72}.[28] In particular, the value of the Sc–S–Sc angle is smaller than those for $Sc_2S@C_s(6)$–C_{82} (114°) and $Sc_2S@C_s(10\,528)$–C_{72} (124°), but similar to that found for $Sc_2S@C_{3v}(8)$–C_{82} (97°). The IPR $Sc_2S@D_{5h}(8149)$–C_{70} is destabilized due to the lack of the metal cation–pentalene interactions. The other non-IPR cages do not possess optimal positioning of the APPs to maximize the metal–pentalene interactions as observed for $Sc_2S@C_2(7892)$–C_{70} (see Fig. 6).

The molar fractions of the lowest-energy $Sc_2S@C_{70}$ isomers as a function of the temperature were also computed using the *rigid rotor and harmonic oscillator* (RRHO) approximation and the related free-encapsulating model (FEM) proposed by Slanina (see Fig. 7).[39,40] Somewhat different results are obtained for the FEM and RRHO approximations. For the FEM, the SCF with cage 7892 is the most abundant isomer in the whole temperature range (to 4000 K). Within the RRHO approximation, there is an isomer preference crossing at around 1700 K, with the IPR isomer predominating at higher temperatures. So far, the predictions derived from the FEM model agree better with experiments than the ones made using the RRHO approximation. In the FEM model we consider that if at high temperature the cluster is rotating freely inside the carbon cages, its contribution to the partition function will be similar for the different cages and will cancel out. In the present case, the Sc_2S will probably rotate inside the spherical IPR cage at sufficiently high temperatures, but it is not so clear that the Sc_2S cluster will freely rotate inside the non-IPR APP2 carbon cage 7892 since the interaction of the Sc ions with the pentalene motifs is significant and there is not a lot of space to rotate inside this cage. The FEM approximation would be the most suitable for the IPR clusterfullerene, but it is not so clear that it would also be the best for the non-IPR 7892 cage, so reality probably lies somewhere between these two approximations. Consequently, we predict $Sc_2S@C_2(7892)$–C_{70} to be the most abundant isomer produced within the temperature range present in the arc.

Good agreement of the computed first and second oxidation and reduction potentials of $Sc_2S@C_2(7892)$–C_{70} with the peaks measured experimentally by cyclic voltammograms reaffirms the assignment, see Table 2. The first anodic potential is predicted to appear at +0.04 V, in good agreement with the experimental half-wave potential (+0.14 V).[41] The predicted first cathodic potential is also close to the experimental value with a difference of around 100 mV (Table 2). The computed electrochemical (EC) gap, 1.37 V, compares reasonably well with experiment, 1.58 V, although the error (210 mV) is somewhat larger than for nitride clusterfullerenes.[41] Inclusion of thermal and entropic effects does not improve the computed gap, as for the family of nitrides.[41] It is worth noting that, for irreversible processes, the comparison between experimental and theoretical electrochemical gaps is difficult, because computations predict standard potentials, and not experimental peak potentials. The predictions for the second anodic and cathodic potentials are in excellent agreement with experiment (with an error of only 50 mV). The HOMO–LUMO gap for the IPR clusterfullerene (0.56 eV) is much smaller than for the 7892 cage (0.95 eV). We have computed the first oxidation potential for $Sc_2S@D_{5h}(8149)$–C_{70} and have found that it is more easily oxidized than $Sc_2S@C_2(7892)$–C_{70} (−0.16 V *vs.* +0.04 V, respectively). We have had problems computing the first reduction potential for $Sc_2S@D_{5h}(8149)$–C_{70} because the LUMO and

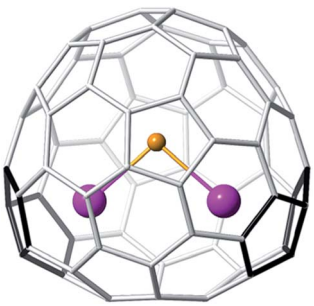

Fig. 6 DFT-optimized structure for $Sc_2S@C_2(7892)$–C_{70}.

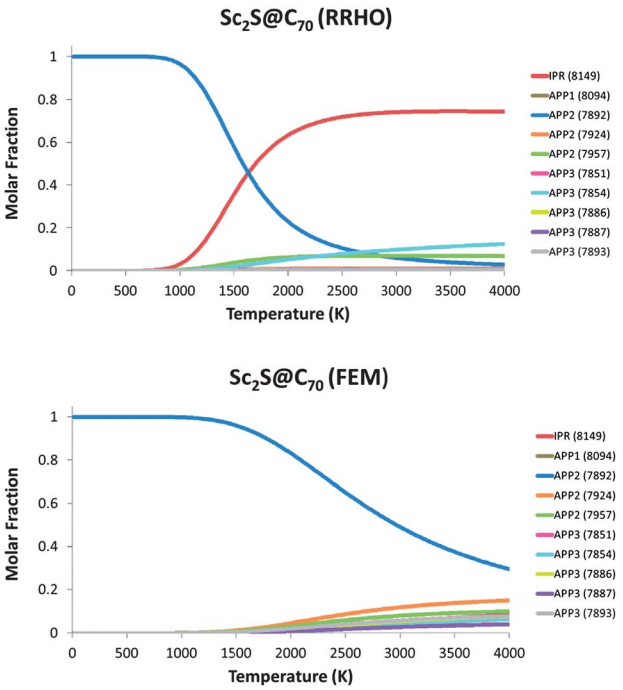

Fig. 7 Predicted molar fractions within the RRHO (top) and FEM (bottom) models as a function of temperature for ten different isomers of $Sc_2S@C_{70}$.

Table 2 Experimental oxidation and reduction potentials (in V *versus* Fc^+/Fc) and computed oxidation and reduction potentials (in V) for $Sc_2S@C_2(7892)$–C_{70}

	O_2	O_1	R_1	R_2	R_3	R_4	EC gap
Exp.	0.65[b]	0.14(70)[a]	−1.44[b]	−1.87[b]	−1.99[b]	−2.45[b]	1.58
Comp.	0.60	0.04	−1.33	−1.82			1.37

[a] Half wave potential. The values in parentheses are the differences between the peak potentials and the half-wave potentials in millivolts. Scan rate, 100 mV s^{-1}. [b] Peak potentials.

LUMO+1 orbitals are almost degenerate and the DFT mono-determinant approach is not suitable to describe such a reduced state (multi-determinant wavefunctions would be needed, but the computational cost is too high for such large systems). According to the energy of the LUMOs ($Sc_2S@D_{5h}(8149)$–C_{70}: −4.04 eV; $Sc_2S@C_2(7892)$–C_{70}: −3.84 eV) the first reduction potential for $Sc_2S@D_{5h}(8149)$–C_{70} should be lower (around 200 mV) than for $Sc_2S@C_2(7892)$–C_{70}, leading to a much smaller EC gap (around 1 eV or even smaller). So, the comparison between computed and experimental electrochemical properties discards $Sc_2S@D_{5h}(8149)$–C_{70} and suggests $Sc_2S@C_2(7892)$–C_{70} as the isomer formed in the arc.

The definitive experiment that confirms isomer 7892 as the carbon cage that encapsulates Sc_2S is the UV-Vis-NIR spectrum. We have computed the spectra using time-dependent (TD) DFT for the two possible SCFs, $Sc_2S@D_{5h}(8149)$–C_{70} and $Sc_2S@C_2(7892)$–C_{70}, in the Vis-NIR region, for wavelengths larger than 500 nm. Despite the systematic underestimation of excitation energies by TD-DFT, this methodology provides a reasonable agreement with experiments for the family of SCFs.[28] From the computations we can clearly discard $Sc_2S@D_{5h}(8149)$–C_{70} because its spectrum shows transitions at large wavelengths (around 1800 and 1600 nm, see Table 3 and ESI†), in total contrast with experimental observations. The spectral onset appears at 1224 nm, see Fig. 3. In addition, the spectrum predicted for $Sc_2S@C_2(7892)$–C_{70} agrees rather well with the experimental one, with the first transition (corresponding to the HOMO–LUMO transition) at 1158 nm (to be compared with the experimental 1102 nm). Therefore, we feel confident that the isolated $Sc_2S@C_{70}$ clusterfullerene corresponds to $Sc_2S@C_2(7892)$–C_{70}.

At this point, it is worth remarking that $C_2(7892)$–C_{70}, the proposed cage for $Sc_2S@C_{70}$, and $C_s(10\,528)$–C_{72}, the one found for $Sc_2S@C_{72}$, are intimately related as the Schlegel diagrams in Fig. 8 show. In fact, cage $C_s(10\,528)$–C_{72} can be obtained by a single C_2 addition to a hexagon of $C_2(7892)$–C_{70} (see ESI†). Therefore, conversion of these two SFCs may happen by single addition/extrusion of a C_2 molecule without further atomic rearrangements. Moreover, it is possible that $Sc_2S@C_s(10\,528)$–C_{72} could form by C_2 addition to $Sc_2S@C_2(7892)$–C_{70} through the recently proposed closed network growth (CNG) mechanism.[42,43]

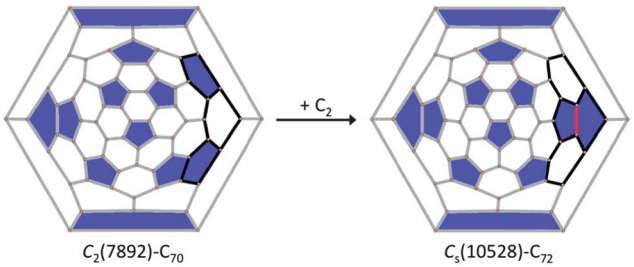

Fig. 8 Schlegel diagrams for cages $C_2(7892)$–C_{70} and $C_s(10\,528)$–C_{72}. The difference between the two cages is highlighted in black with the added C_2 unit in red. The larger distance between the two APPs in cage $C_s(10\,528)$–C_{72} compared to that for $C_2(7892)$–C_{70} makes the Sc–S–Sc angle in $Sc_2S@C_s(10\,528)$–C_{72} (124°) larger than that found for $Sc_2S@C_2(7892)$–C_{70} (98°).

Beside $Sc_2S@C_2(7892)$–C_{70}, only one non-IPR C_{70} endohedral fullerene, $Sc_3N@C_{2v}(7854)$–C_{70}, has been reported so far. Very recently, Nagase, Zhao and co-workers proposed, using density functional theory, that $Sc_2@C_{2v}(7854)$–C_{70} and not the corresponding carbide, $Sc_2C_2@C_{2v}(6073)$–C_{68}, is the metallofullerene detected as Sc_2C_{70}.[44] These two isomers, $C_2(7892)$–C_{70} and $C_{2v}(7854)$–C_{70}, are rather close in energy when computed as tetraanions (Table 4). On the other hand, the hexaanionic state is much more favored for $C_{2v}(7854)$–C_{70}. If the trapped cluster is Sc_3N, a six electron transfer combined with the optimal interaction between the three Sc atoms and the three pentalenes on cage $C_{2v}(7854)$–C_{70} (Fig. 9) lead to the preferential stabilization of $Sc_3N@C_{2v}(7854)$–C_{70}, as proposed by Yang *et al.*[30] (Table 4). However, with the Sc_2S cluster inside the Sc–pentalene interactions are optimized for $Sc_2S@C_2(7892)$–C_{70}, which has, by far, the lowest energy (Tables 1 and 4). Although sharing the same cage size, the number and the position of the pentalene motifs are significantly different in these two isomers. This shows that the nature and geometry of the encaged cluster plays an important role on the selection of the cage isomer, along with the electronic stabilization resulting from cluster–cage electron transfer.

Table 3 TDDFT predictions for the most intense lowest-energy excitations in the absorption spectrum of $Sc_2S@C_2(7892)$–C_{70} and $Sc_2S@D_{5h}(8149)$–C_{70}

E (eV)	λ (nm)	f^a	Leading configurations[b] (%)
$Sc_2S@C_2(7892)$–C_{70}			
1.071	1158	0.00650	HOMO → LUMO (98)
1.212	1023	0.00356	HOMO → LUMO+1 (98)
1.664	745	0.00104	HOMO → LUMO+3 (99)
1.681	738	0.00519	HOMO → LUMO+4 (96)
1.853	669	0.00721	HOMO-1 → LUMO (89)
$Sc_2S@D_{5h}(8149)$–C_{70}			
0.688	1802	0.00365	HOMO → LUMO (63); HOMO → LUMO+1 (36)
0.763	1625	0.00103	HOMO-1 → LUMO+1 (63); HOMO-1 → LUMO (26)
0.802	1546	0.00715	HOMO-1 → LUMO (71); HOMO-1 → LUMO+1 (28)
0.980	1265	0.00138	HOMO → LUMO+2 (50); HOMO-1 → LUMO+3 (47)
1.295	958	0.05558	HOMO-1 → LUMO+3 (46); HOMO → LUMO+2 (35)

[a] Only excitations with f (oscillator strength) > 0.001 are listed. [b] Contributions less than 10% are omitted.

Table 4 Relative energies (in kcal mol^{-1}) for cages C_2(7892)–C_{70} and C_{2v}(7854)–C_{70} in different anionic states and encapsulating different clusters

	C_2(7892)–C_{70}	C_{2v}(7854)–C_{70}
C_{70}^{4-}	0.0	4.6
C_{70}^{6-}	16.2	0.0
$Sc_2S@C_{70}$	0.0	26.3
$Sc_3N@C_{70}$[a]	10.5	0.0

[a] The stabilization of cage C_{2v}(7854)–C_{70} *vs.* C_2(7892)–C_{70} (10.5 kcal mol^{-1}) is smaller than for the corresponding hexaanions (16.2 kcal mol^{-1}) due to larger structural distortions of the Sc_3N cluster inside the C_{2v}(7854)–C_{70} cage (see Fig. 9 and ESI†).

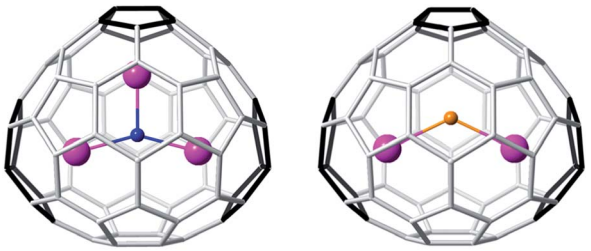

Fig. 9 DFT-optimized structures for $Sc_3N@C_{2v}$(7854)–C_{70} and $Sc_2S@C_{2v}$(7854)–C_{70}.

Conclusions

In summary, a new isomer of C_{70}, $Sc_2S@C_2$(7892)–C_{70}, has been isolated and characterized by mass spectrometry, UV-Vis-NIR absorption spectroscopy, cyclic voltammetry and DFT calculations. The combined experimental and computational studies led to the unambiguous assignment of the cage symmetry to C_2(7892)–C_{70}, the second non-IPR isomer of C_{70} to be detected experimentally. $Sc_2S@C_2$(7892)–C_{70} is by far the lowest-energy isomer and the major candidate to be the experimentally detected $Sc_2S@C_{70}$. At high temperatures, isomer $Sc_2S@D_{5h}$(8149)–C_{70} could also be formed, but comparison of the experimental and theoretical electrochemical properties and UV-Vis-NIR spectra clearly discards the IPR $Sc_2S@D_{5h}$(8149)–C_{70}. Cage C_2(7892)–C_{70} is structurally intimately related to cage C_s(10 528)–C_{72}, the one that has been recently detected by single crystal X-ray crystallography for $Sc_2S@C_{72}$. Thus, besides $Sc_2S@C_s$(10 528)–C_{72}, $Sc_2S@C_2$(7892)–C_{70} provides an additional example of stabilization of a new non-IPR cage resulting from the combined effect of a four-electron transfer and the unique geometrical fit between the Sc_2S cluster and the cage. Many more structures and interesting properties are yet to be explored in the SCF family.

Acknowledgements

We thank the Robert A. Welch Foundation for an endowed chair, grant #AH-0033 and the US NSF for grant CHE-1110967, which provided generous support for this work. This work is also supported by the Spanish Ministry of Science and Innovation (Project no. CTQ2011-29054-C02-01) and by the Generalitat de Catalunya (2009SGR462 and XRQTC). Additional support from the US NSF, grant CHE-1124075 and from the Spanish Ministry of Science and Innovation (PRI-PIBUS-2011-0995) for a joint US-Spain collaboration is also acknowledged.

Notes and references

§ The calculations were carried out by using DFT methodology with the ADF 2010 package.[45,46] The exchange-correlation functionals of Becke and Perdew were used.[47,48] Relativistic corrections were included by means of the ZORA formalism. Slater triple-zeta polarization basis sets were employed to describe the valence electrons of C, S and Sc. Frozen cores consisting of the 1s shell for C and the 1s and 2p shells for S and Sc were described by means of single Slater functions. The computational study of the UV-Vis-NIR spectra has been performed using TDDFT methodology (also at BP86/TZP level).

1 H. W. Kroto, J. R. Heath, S. C. O'Brien, R. F. Curl and R. E. Smalley, *Nature*, 1985, **318**, 162–163.
2 A. Rodriguez-Fortea, S. Irle and J. M. Poblet, *Wiley Interdiscip. Rev.: Comput. Mol. Sci.*, 2011, **1**, 350–367.
3 H. Shinohara, *Rep. Prog. Phys.*, 2000, **63**, 843–892.
4 T. Akasaka and S. Nagase, *Endofullerenes: A New Family of Carbon Clusters*, Kluwer Academic Publishers, Dordrecht, Boston, 2002.
5 S. Yang, F. Liu, C. Chen, M. Jiao and T. Wei, *Chem. Commun.*, 2011, **47**, 11822–11839.
6 L. Dunsch and S. Yang, *Phys. Chem. Chem. Phys.*, 2007, **9**, 3067–3081.
7 A. Rodriguez-Fortea, A. L. Balch and J. M. Poblet, *Chem. Soc. Rev.*, 2011, **40**, 3551–3563.
8 S. Stevenson, G. Rice, T. Glass, K. Harich, F. Cromer, M. R. Jordan, J. Craft, E. Hadju, R. Bible, M. M. Olmstead, K. Maitra, A. J. Fisher, A. L. Balch and H. C. Dorn, *Nature*, 1999, **401**, 55–57.
9 L. Dunsch and S. Yang, *Small*, 2007, **3**, 1298–1320.
10 C. R. Wang, T. Kai, T. Tomiyama, T. Yoshida, Y. Kobayashi, E. Nishibori, M. Takata, M. Sakata and H. Shinohara, *Angew. Chem., Int. Ed.*, 2001, **40**, 397–399.
11 T. S. Wang, N. Chen, J. F. Xiang, B. Li, J. Y. Wu, W. Xu, L. Jiang, K. Tan, C. Y. Shu, X. Lu and C. R. Wang, *J. Am. Chem. Soc.*, 2009, **131**, 16646–16647.
12 S. Stevenson, M. A. Mackey, M. A. Stuart, J. P. Phillips, M. L. Easterling, C. J. Chancellor, M. M. Olmstead and A. L. Balch, *J. Am. Chem. Soc.*, 2008, **130**, 11844–11845.
13 R. Valencia, A. Rodríguez-Fortea, S. Stevenson, A. L. Balch and J. M. Poblet, *Inorg. Chem.*, 2009, **48**, 5957–5961.
14 B. Q. Mercado, M. M. Olmstead, C. M. Beavers, M. L. Easterling, S. Stevenson, M. A. Mackey, C. E. Coumbe, J. D. Phillips, J. P. Phillips, J. M. Poblet and A. L. Balch, *Chem. Commun.*, 2010, **46**, 279–281.
15 L. Dunsch, S. Yang, L. Zhang, A. Svitova, S. Oswald and A. A. Popov, *J. Am. Chem. Soc.*, 2010, **132**, 5413–5421.
16 N. Chen, M. N. Chaur, C. Moore, J. R. Pinzon, R. Valencia, A. Rodriguez-Fortea, J. M. Poblet and L. Echegoyen, *Chem. Commun.*, 2010, **46**, 4818–4820.
17 B. Q. Mercado, N. Chen, A. Rodríguez-Fortea, M. A. Mackey, S. Stevenson, L. Echegoyen, J. M. Poblet, M. M. Olmstead and A. L. Balch, *J. Am. Chem. Soc.*, 2011, **133**, 6752–6760.
18 N. Martin, *Chem. Commun.*, 2006, 2093–2104.

19 S. Laus, B. Sitharaman, É. Tóth, R. D. Bolskar, L. Helm, S. Asokan, M. S. Wong, L. J. Wilson and A. E. Merbach, *J. Am. Chem. Soc.*, 2005, **127**, 9368–9369.
20 E. Toth, R. D. Bolskar, A. Borel, G. Gonzalez, L. Helm, A. E. Merbach, B. Sitharaman and L. J. Wilson, *J. Am. Chem. Soc.*, 2005, **127**, 799–805.
21 S. Sato, S. Seki, G. Luo, M. Suzuki, J. Lu, S. Nagase and T. Akasaka, *J. Am. Chem. Soc.*, 2012, **134**, 11681–11686.
22 L. Feng, M. Rudolf, S. Wolfrum, A. Troeger, Z. Slanina, T. Akasaka, S. Nagase, N. Martín, T. Ameri, C. J. Brabec and D. M. Guldi, *J. Am. Chem. Soc.*, 2012, **134**, 12190–12197.
23 S. Sato, S. Seki, Y. Honsho, L. Wang, H. Nikawa, G. Luo, J. Lu, M. Haranaka, T. Tsuchiya, S. Nagase and T. Akasaka, *J. Am. Chem. Soc.*, 2011, **133**, 2766–2771.
24 J. R. Pinzon, M. E. Plonska-Brzezinska, C. M. Cardona, A. J. Athans, S. S. Gayathri, D. M. Guldi, M. A. Herranz, N. Martin, T. Torres and L. Echegoyen, *Angew. Chem., Int. Ed.*, 2008, **47**, 4173–4176.
25 R. B. Ross, C. M. Cardona, D. M. Guldi, S. G. Sankaranarayanan, M. O. Reese, N. Kopidakis, J. Peet, B. Walker, G. C. Bazan, E. Van Keuren, B. C. Holloway and M. Drees, *Nat. Mater.*, 2009, **8**, 208–212.
26 R. B. Ross, C. M. Cardona, F. B. Swain, D. M. Guldi, S. G. Sankaranarayanan, E. V. Keuren, B. C. Holloway and M. Drees, *Adv. Funct. Mater.*, 2009, **19**, 2332–2337.
27 E.-Y. Zhang, C.-Y. Shu, L. Feng and C.-R. Wang, *J. Phys. Chem. B*, 2007, **111**, 14223–14226.
28 N. Chen, C. M. Beavers, M. Mulet-Gas, A. Rodríguez-Fortea, E. J. Munoz, Y.-Y. Li, M. M. Olmstead, A. L. Balch, J. M. Poblet and L. Echegoyen, *J. Am. Chem. Soc.*, 2012, **134**, 7851–7860.
29 W. Kratschmer, L. D. Lamb, K. Fostiropoulos and D. R. Huffman, *Nature*, 1990, **347**, 354–358.
30 S. F. Yang, A. A. Popov and L. Dunsch, *Angew. Chem., Int. Ed.*, 2007, **46**, 1256–1259.
31 M. N. Chaur, F. Melin, A. L. Ortiz and L. Echegoyen, *Angew. Chem., Int. Ed.*, 2009, **48**, 7514–7538.
32 B. Q. Mercado, M. A. Stuart, M. A. Mackey, J. E. Pickens, B. S. Confait, S. Stevenson, M. L. Easterling, R. Valencia, A. Rodriguez-Fortea, J. M. Poblet, M. M. Olmstead and A. L. Balch, *J. Am. Chem. Soc.*, 2010, **132**, 12098–12105.
33 B. Q. Mercado, N. Chen, A. Rodriguez-Fortea, M. A. Mackey, S. Stevenson, L. Echegoyen, J. M. Poblet, M. M. Olmstead and A. L. Balch, *J. Am. Chem. Soc.*, 2011, **133**, 6752–6760.
34 A. Rodriguez-Fortea, N. Alegret, A. L. Balch and J. M. Poblet, *Nat. Chem.*, 2010, **2**, 955–961.
35 P. W. Fowler and D. E. Manolopoulos, *An Atlas of Fullerenes*, Oxford University Press, Oxford, 1995.
36 S. Stevenson, P. W. Fowler, T. Heine, J. C. Duchamp, G. Rice, T. Glass, K. Harich, E. Hajdu, R. Bible and H. C. Dorn, *Nature*, 2000, **408**, 427–428.
37 B. Q. Mercado, C. M. Beavers, M. M. Olmstead, M. N. Chaur, K. Walker, B. C. Holloway, L. Echegoyen and A. L. Balch, *J. Am. Chem. Soc.*, 2008, **130**, 7854.
38 T. Zuo, K. Walker, M. M. Olmstead, F. Melin, B. C. Holloway, L. Echegoyen, H. C. Dorn, M. N. Chaur, C. J. Chancellor, C. M. Beavers, A. L. Balch and A. J. Athans, *Chem. Commun.*, 2008, 1067–1069.
39 Z. Slanina, S. L. Lee, F. Uhlik, L. Adamowicz and S. Nagase, *Theor. Chem. Acc.*, 2007, **117**, 315–322.
40 Z. Slanina and S. Nagase, *ChemPhysChem*, 2005, **6**, 2060–2063.
41 R. Valencia, A. Rodriguez-Fortea, A. Clotet, C. de Graaf, M. N. Chaur, L. Echegoyen and J. M. Poblet, *Chem.–Eur. J.*, 2009, **15**, 10997–11009.
42 P. W. Dunk, N. K. Kaiser, C. L. Hendrickson, J. P. Quinn, C. P. Ewels, Y. Nakanishi, Y. Sasaki, H. Shinohara, A. G. Marshall and H. W. Kroto, *Nat. Commun.*, 2012, **3**, 855.
43 P. W. Dunk, N. K. Kaiser, M. Mulet-Gas, A. Rodriguez-Fortea, J. M. Poblet, H. Shinohara, C. L. Hendrickson, A. G. Marshall and H. W. Kroto, *J. Am. Chem. Soc.*, 2012, **134**, 9380–9389.
44 H. Zheng, X. Zhao, W.-W. Wang, T. Yang and S. Nagase, *J. Chem. Phys.*, 2012, **137**, 014308.
45 A. Osterholm, A. Petr, C. Kvarnstrom, A. Ivaska and L. Dunsch, *J. Phys. Chem. B*, 2008, **112**, 14149–14157.
46 G. T. Velde, F. M. Bickelhaupt, E. J. Baerends, C. F. Guerra, S. J. A. Van Gisbergen, J. G. Snijders and T. Ziegler, *J. Comput. Chem.*, 2001, **22**, 931–967.
47 A. D. Becke, *Phys. Rev. A: At., Mol., Opt. Phys.*, 1988, **38**, 3098–3100.
48 J. P. Perdew, *Phys. Rev. B*, 1986, **33**, 8822–8824.

